ANN Modeling of Thermal Conductivity and Viscosity of MXene-Based Aqueous IoNanofluid

Naman Parashar[1] · Navid Aslfattahi[2] · Syed Mohd Yahya[1] · R. Saidur[3,4]

[1] Sustainable Energy & Acoustics Research Lab, Mechanical Engineering Department, AMU, Aligarh 202002, India

[2] Department of Mechanical Engineering, Faculty of Engineering, University of Malaya, Kuala Lumpur 50603, Malaysia

[3] Research Center for Nano-Materials and Energy Technology (RCNMET), School of Science and Technology, Sunway University, Bandar Sunway, 47500 Petaling Jaya, Selangor Darul Ehsan, Malaysia

[4] Department of Engineering, Lancaster University, Lancaster LA1 4YW, UK

Abstract

Research shows that due to enhanced properties IoNanofluids have the potential of being used as heat transfer fluids (HTFs). A significant amount of experimental work has been done to determine the thermophysical and rheological properties of IoNanofluids; however, the number of intelligent models is still limited. In this work, we have experimentally determined the thermal conductivity and viscosity of MXene-doped [MMIM][DMP] ionic liquid. The size of the MXene nanoflakes was determined to be less than 100 nm. The concentration was varied from 0.05 mass% to 0.2 mass%, whereas the temperature varied from 19 °C to 60 °C. The maximum thermal conductivity enhancement of 1.48 was achieved at 0.2 mass% and 30 °C temperature. For viscosity, the maximum relative viscosity of 1.145 was obtained at 0.2 mass% and 23 °C temperature. After the experimental data for thermal conductivity and viscosity were obtained, two multiple linear regression (MLR) models were developed. The MLR models' performances were found to be poor, which further called for the development of more accurate models. Then two feedforward multilayer perceptron models were developed. The Levenberg–Marquardt algorithm was used to train the models. The optimum models had 4 and 10 neurons for thermal conductivity and viscosity model, respectively. The values of statistical indices showed the models to be well-fit models. Further, relative deviations values were also accessed for training data and testing data, which further showed the models to be well fit.

Keywords Aqueous ionic liquid · 1,3-Dimethyl imidazolium dimethyl-phosphate · Levenberg–Marquardt algorithm · MXene · Thermal conductivity · Viscosity

Abbreviations

HTF	Heat transfer fluid
IL	Ionic liquid
NEIL	Nanoparticle-enhanced ionic liquid
INF	IoNanofluid
MWCNTs	Multiwalled carbon nanotubes
GNP	Graphene nanoplatelets
EG	Ethylene glycol
ANFIS	Adaptive neuro fuzzy inference system
ARD	Average relative deviation
ANN	Artificial neural network
SVR	Support vector regression
MLR	Multiple linear regression
LM	Levenberg–Marquardt
MSE	Mean square error
MAE	Mean absolute error
RD	Relative deviation
TCR	Thermal conductivity ratio
RV	Relative viscosity

1 Introduction

With rapid advancements in the energy sector, increasing the efficiency of the heat transfer process has become a need of the hour. For a very long time, fluids such as water, ethylene glycol, oil, *etc*. have been used as heat transfer fluids (HTFs) and coolants in various industries. However, due to low thermal conductivity, these fluids have limitations in terms of how efficiently they can remove the heat. This, in turn, puts limitations on the efficiency of heat transfer systems. Although several methods can be applied to increase the heat transfer capability of a system [1, 2], the fundamental problem remains unsolved, *i.e.*, the low heat transfer capability of fluids. This problem was solved efficiently when, for the first time, nanofluid was developed by Choi and Eastman [3]. Nanofluids are the fluids which are enhanced with nanomaterials (*i.e.*, nanoparticles, nanotubes, nanoflakes, nanofibers). These nanomaterial-enhanced fluids due to their enhanced properties have the potential of being used as heat transfer fluids (HTFs) in a wide range of applications [4–6]. However, nanofluids also have some drawbacks. One such drawback is the low dispersion stability of nanomaterials in the base fluids [7, 8]. These drawbacks encouraged researchers to look for other fluids that may have the potential of being used as heat transfer fluids (HTFs).

Ionic liquid (IL), which consists of cations and anions, is a relatively new class of organic liquids that stays in liquid form at room temperature and/or have melting point below 100 °C [9]. Ionic liquids are known to have very low vapor pressure, negligible-volatility, high viscosity, and good thermal stability at high temperatures [10–12]. Moreover, ILs are also known for their tunable properties [12, 13]. These excellent properties of ILs have resulted into their wide applications such as catalytic [14, 15], synthesis [16], electrochemistry [17], heat transfer systems [18, 19],

and energy storage [20]. It is estimated that by combining different anions and cations, over 10^{18} different ternary ILs can be formed [11].

The doping of various nanomaterial structures in ILs is a way to further enhance their properties. ILs when suspended with these nanomaterial structures are known as nanoparticle-enhanced ionic liquids (NEILs) or IoNanofluids (INFs). IoNanofluids are known to have shown better thermal conductivity, heat transfer properties, *etc.* when compared to conventional ILs. Hence with these improved properties of INFs, they have the potential of being used as heat transfer fluids (HTFs) [21–25].

Various researchers and scholars have conducted a good number of studies on the thermophysical properties of INFs. Cherecheş *et al.* [26] studied thermophysical properties of different aqueous INFs. The INFs were prepared by dispersing different concentrations of alumina (Al_2O_3) nanoparticles in different mixtures of water and [C_2mim][CH_3SO_3] ionic liquid. The value of pH for all the IoNanofluids was found to be in the 8.0–8.5 range, which indicated their good stability. The maximum enhancement of 12.9 % was reported in thermal conductivity at the conditions of 15 mass% concentration and 293.15 K temperature. Paul *et al.* [27] studied density, thermal conductivity, viscosity, heat capacity, and heat transfer coefficient for Al_2O_3 nanoparticle-doped [C_4mim][NTf_2] ionic liquid. A strong shear thinning behavior was reported at 0.9 vol% concentration. Besides, the viscosity was also found to be significantly higher than that of the pure ionic liquid. The thermal conductivity and heat capacity enhancement of 11 % and 49 % was reported at 0.9 vol% concentration. The convective heat transfer coefficient was reported to be more for IoNanofluid. Further, enhancement in the convective heat transfer was also shown to be more for turbulent flow when compared to laminar flow.

Paul *et al.* [28], in another study, studied thermal conductivity, heat capacity, heat transfer performance of Al_2O_3 nanoparticle (1 mass%)-enhanced [C_4mpyrr][NTf_2] and [C_4mim][NTf_2] ionic liquids. In the study, thermal conductivity enhancement of 6 % and 5 % was reported for [C_4mim][NTf_2] and [C_4mpyrr][NTf_2], respectively. Moreover, enhancement of 23 % and 20 % was reported in the heat capacity and heat transfer coefficient, respectively. Nieto de Castro *et al.* [2] studied thermal conductivity and heat capacity for Imidazolium and Pyrrolidinium ionic liquids enhanced with multiwalled carbon nanotubes (MWCNTs). In the study, thermal conductiv- ity enhancement of 2 % to 9 % and heat capacity enhancement of up to 8 % was reported. Recently, Zhang *et al.* [22] studied thermal stability, viscosity, thermal conductivity, and specific heat capacity of graphene nanoplatelets (GNPs)-sus- pended [EMIm]Ac ionic liquid. The maximum viscosity and thermal conductivity enhancement of 27.7 % and 43.3 % was reported at the temperature of 373.15 K and GNP concentration of 5 mass%. The maximum reduction of 3.62 % was also reported in specific heat capacity at the same temperature and GNP concentration. Furthermore, an increase of 28.6 % was also reported in the heat transfer coefficient at 5 mass% concentration.

Wang *et al.* [29] studied viscosity, specific heat, and thermal conductivity of graphene and MWCNTs-enhanced [HMIM]BF_4 ionic liquid. For a given nanomaterial concentration, enhancement in the thermal conductivity was found to be greater for graphene INF. For graphene INF, a maximum thermal conductivity enhancement of 18.6 % was reported at the conditions of 0.06 mass% concentration and 65 ℃

temperature. The INFs were also found to be showing lower specific heat when compared to pure ionic liquids. Moreover, specific heat was found to be lower for graphene INFs, which decreased even further as graphene loading increased. Furthermore, viscosity of the graphene-based INF was found to be higher than that of the MWCNTs-based INF. Xie *et al*. [30] studied thermal conductivity, density and viscosity of [EMIM][DEP] and its water solution enhanced with MWCNTs nanomaterials. A maximum thermal conductivity enhancement of 9.7 % was reported in the study. Moreover, viscosity was reported to increasing with increase in MWCNTs concentration and decreasing with increase in temperature.

MXene is a relatively new class of 2-dimensional inorganic material having many attractive properties and applications in number of fields [31]. Moreover, properties of MXene can be tuned by altering composition and morphology [31]. However, MXene is relatively unexplored in the field of nanofluids. Bao *et al*. [32] determined the thermophysical properties of MXene/EG nanofluid. In the study, multilayer and single-layer MXene nanomaterials were suspended in EG. They reported maximum thermal conductivity enhancement of 64.9 % for single-layer MXene at 5 vol%. Besides, viscosity of MXene-based EG nanofluid was also found to be lower than that of the graphene and MWCNTs-based EG nanofluid. Moreover, single-layer MXene nanofluid was found to be stable for a period of over 30 days. Aslfattahi *et al*. [33] studied the effect of MXene/silicone oil nanofluid on the performance of concentrated solar photovoltaic thermal collector. In the study, viscosity of the newly developed nanofluid was also studied. Generally, with the addition of nanoparticles, viscosity of nanofluids increases. However, in this study, viscosity of the nanofluid was found to be independent of the MXene concentration. Furthermore, at the conditions of 150 °C temperature and 0.1 mass% MXene concentration, enhancement of around 64 % was observed in the thermal conductivity. These studies reporting low viscosity and high thermal conductivity of MXene-based nanofluids coupled with good properties of MXene paves the way for developing more MXene-based nanofluids and IoNanofluids.

Most of the researchers and scholars have only presented experimental values of thermophysical and rheological properties of INFs. This increases the cost and consumes time as well. Developing models can be a good way to eliminate or reduce the need of carrying out experiments [34]. Maryam Sadi [35] developed an adap- tive neuro fuzzy inference system (ANFIS) to predict the thermal conductivity and viscosity of different INFs. The temperature, nanoparticle concentration, and ionic liquid molecular weight were given as inputs to the model. The model developed for thermal conductivity and viscosity showed good performance. The values of average relative deviation (ARD) and coefficient of determination (R^2) for thermal conductivity model were 0.72 % and 0.9959, respectively. For viscosity model, these values were 5.1 % and 0.9934, respectively.

As presented, significant work on the experimental determination of INFs' thermophysical and rheological properties has been done, but models available in the literature that can be used to predict the values of these properties are limited. Machine learning techniques such as artificial neural networks (ANNs), ANFIS, support vector regression (SVR) models are great tools for regression analysis which can be used to predict the thermal conductivity and viscosity of IoNanofluids. Therefore,

Table 1 The specifications of MXene nanomaterials

Chemical formula	Appearance	Density (kg/m^3)	Thermal conductivity (W/m-K)	Size (nm)
Ti_3C_2	Black	3700	55.8	< 100

Table 2 The thermophysical and rheological properties of ionic liquid and water (at 20 °C)

	Purity (%)	Thermal conductivity (W/m-K)	Density (kg/m^3)	Viscosity (mPas)	Color
Ionic Liquid	≥ 98	0.468	1270	1.6	Yellow
Water	≥ 99.998	0.6	997	0.89	Colorless

in this work, feedforward neural network models were developed to predict the values of thermal conductivity and viscosity of MXene-based aqueous INF. To prepare the INF, MXene nanomaterial was first synthesized and then dispersed in aqueous [MMIM][DMP] ionic liquid. To develop the models, thermal conductivity and viscosity values were first determined experimentally for 0.05, 0.1, and 0.2 mass% concentration and wide range of temperature. Besides, two multiple linear regression (MLR) models were also developed in the work.

2 Materials and Method

2.1 Materials

The ionic liquid (IL) 1,3-Dimethylimidazolium dimethyl-phosphate [MMIM] [DMP] with purity of ≥ 98 % and density of 1.27 g/cm^3 was supplied by Merck KGaA, Darmstadt, Germany. The MAX phase (Ti_3AlC_2) procurement was through Y.Carbon Ltd company. All the materials were used as received without any further purification. The specifications of MXene and base fluids are shown in Tables 1 and 2, respectively.

The process of synthesis of MXene nanoflakes has already been described in other work of the authors [36]. In the work, performance of hybrid solar PV/T sys- tem was analyzed for MXene-aqueous IoNanofluid.

2.2 FESEM Analysis of Synthesized MXene Nanoflakes

Morphological analysis of the MXene (Ti_3C_2) nanoflakes was conducted by high-resolution FESEM (JEOL, JSM-7800F). Stacking of several MXene sheets oriented as flake structures disclose the effective exfoliation of Ti_3C_2 MXene from the precursor Ti_3AlC_2 MAX phase. Figure 1 shows the FESEM image of the synthesized MXene nanomaterials. The size of the MXene nanoflakes was found to be less than 100 nm.
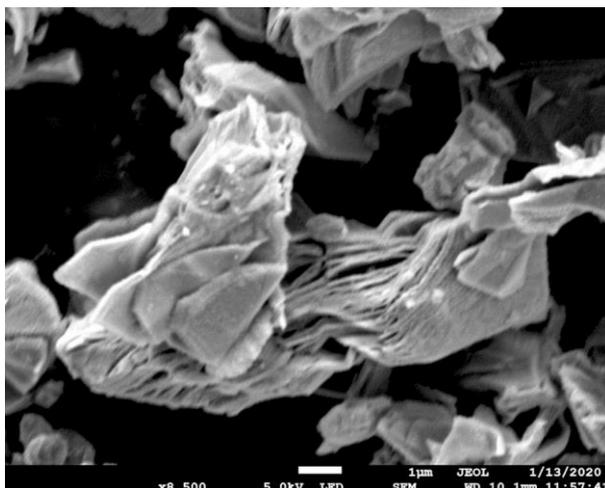
Fig. 1 FESEM analysis of the synthesized MXene nanomaterials at 1 µm magnification

2.3 Preparation of MXene-Enhanced 1,3-Dimethyl Imidazolium Dimethyl-Phosphate Ionic Liquid (IoNanofluids)

The aqueous solution of ionic liquid was prepared with ratio of 20 vol% of [MMIM] [DMP] and 80 vol% of deionized water. Firstly, 20 ml of IL was added to the beaker followed by adding 80 ml of deionized water. Acquired 100 ml of the aqueous solution of IL was weighed using microbalance (TX323L, UNIBLOC) to calculate the amount of MXene in terms of weight percentage. IoNanofluids were prepared in three different loading concentrations of 0.05 mass%, 0.1 mass%, and 0.2 mass% MXene nanoflakes. For the preparation of IoNanofluids, the pre-defined amount of MXene nanoflakes was added to the IL solution, followed by stirring for 1 h at 50 °C and 700 rpm using hot plate magnet stirrer (RCT basis). The resultant solution was probe sonicated (Fs-1200N) for 30 min with power of 70 % and on/off time of 7/3 s. Finally, a stable and well-dispersed IoNanofluid solution was prepared successfully.

2.4 Thermal Conductivity and Viscosity Measurement of IoNanofluid

The thermal conductivity measurement was performed using thermal properties analyzer. The measurement was conducted for 0.05 mass%, 0.1 mass%, and 0.2 mass% MXene concentration and 25 °C to 60 °C temperature.

The viscosity measurement was performed using Rheometer Anton Paar (MCR92). T-Ramp measurement (viscosity as a function of temperature) was performed for the aqueous solution of IL and IL/MXene IoNanofluids at different concentrations consisting of 0.05 mass%, 0.1 mass%, and 0.2 mass% in the temperature range of 19.14 °C to 50.15 °C.

Table 3 shows the details of thermal conductivity and viscosity instrument's accuracy and uncertainty.

Table 3 The accuracy and uncertainty of thermal conductivity and viscosity measuring instrument

Parameters	Measuring instrument	Accuracy (%)	Uncertainty (%)
Thermal conductivity	Thermal property 198 analyzer (Model: Tempos)	±10	1.5–5
Viscosity	Rheometer (Anton Par, Model: MCR 92)	± 1.0	2–6.6

3 Levenberg–Marquardt Feedforward Neural Network

Artificial neural network (ANN) is a type of soft computational model inspired by the working of neurons in the brain. ANNs make use of concepts of algebra, calculus, statistics, and probability to learn the mapping between input variables and output variables. The building block of ANNs is known as neuron, where all the calculations take place. These neurons have some weights and biases associated with them. The structure of a typical ANN and neuron working is shown in Fig. 2. It shows a structure with 3 input parameters, 4 hidden neurons, and 1 output param- eter. In the figure, $X1$, $X2$, and $X3$ are the inputs to the hidden neuron and $w1$, $w2$, and $w3$ are the weights associated with a hidden neuron. The sigma sign denotes the weighted sum of inputs, f denotes the activation function used, and Y represents the output of a neuron.

As ANNs are not programmed to solve a specific problem only, they need to be trained for any particular problem. The training is a process of finding the values of weights and biases that reduces the error between original values and predicted
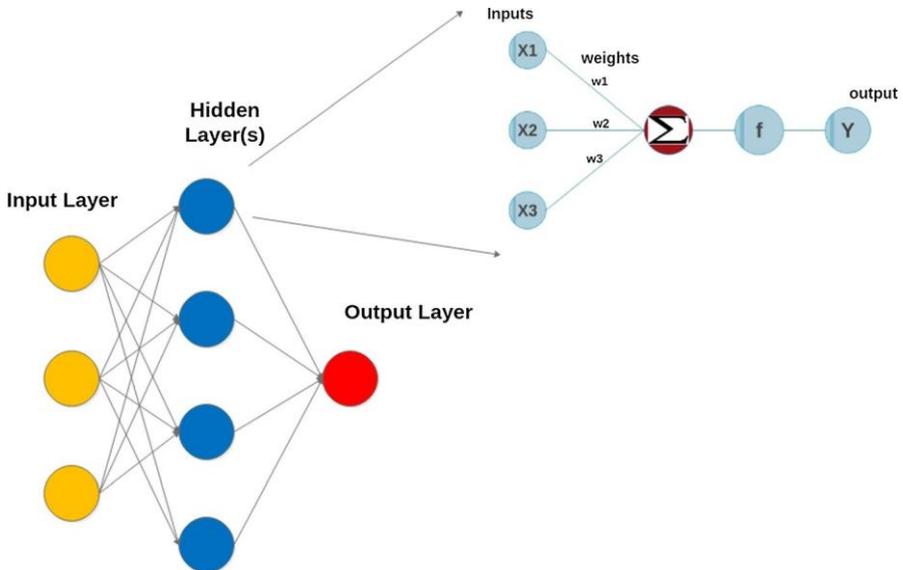
Fig. 2 The structure of a typical ANN model and working of a neuron

values to the least possible value. Various algorithms that are used to train the neural networks are gradient descent [46], Gauss–Newton method, Levenberg–Mar- quardt [37], *etc*. Optimization algorithms such as genetic algorithm [38, 39], particle swarm optimization [40], ant colony optimization [41] are also commonly used. In this work, Levenberg–Marquardt (LM) algorithm is used. The LM algorithm can be viewed as the combination of gradient descent algorithm and Gauss–Newton algorithm. This means that when the errors are large, LM works as gradient descent algorithm, and when errors are small, it works as Gauss–Newton algorithm. The LM algorithm is faster (unlike gradient descent) and usually converges to optimum solu- tion even if initial approximation is far from optimum solution (unlike Gauss–New- ton). This algorithm is also known as least square algorithm and usually gives better performance than other optimization algorithms. In this work, the optimum topol- ogy of the models was found through trial and error method.

3.1 Data Analysis

Table 4 shows the statistical details of the experimentally obtained values of viscos- ity and thermal conductivity.

The table shows the value of skewness, kurtosis, and correlation coefficient with output variable. The skewness value shows the distribution of the data. A skewness value close to 0 indicates the normal distribution of the variable. Any data is said to be reasonably symmetrical if the skewness value lies between − 0.5 and 0.5. There- fore, it can be seen from the table that the distribution of all the variables is fairly symmetrical. The kurtosis value tells about the outliers in the data. The performance of neural networks is known to be affected by outliers. A normal distribution will have value of kurtosis as 3. A value greater than 3 shows the presence of outliers and a value smaller than 3 shows the absence of outliers. Therefore, it can be deduced from the table that all the variables are close to being normally distributed and have no outliers. These two statistical values (skewness and kurtosis) can help analyze the variation of errors with various variables. The correlation coefficient gives out infor- mation regarding the relationship between variables. A negative value indicates an inverse relationship; a positive value indicates a direct relationship; 0 value indicates no relationship. Also, for perfectly linearly correlated variables, the value of the cor- relation coefficient is either 1 or − 1. Therefore, it can be seen from the table that viscosity has near linear relationship with temperature, whereas other parameters have non-linear relationships with outputs. Further, the table also shows the mini- mum and maximum values of all variables. It can be seen that different variables have values in different scales. In such cases, it is a common practice to transform the variables to a common range. Hence, the data were transformed in the range of 0 to 1 by using following relation:

$$V_{norm} = \frac{V - V_{min}}{V_{max} - V_{min}} \tag{1}$$

where V, V, V_{min}, and V represent normalized value, actual experimental value, minimum value, and maximum value of the variables.

Table 4 The statistical details of the experimentally determined data

	Parameter	Unit	Minimum value	Maximum value	Skewness value	Kurtosis value	Correlation with output
Viscosity	Input	°C	19.14	50.15	− 0.1199	1.807	− 0.94
		mass%	0	0.2	0.43465	1.8457	0.26
	Output	mPa·s	2.0234	3.0964	0.41625	1.937	1
Thermal conductivity	Input	˚C	25	60	− 0.173	2.180	0.44
		mass%	0	0.2	0.43465	1.8457	0.82
	Output	W/m-K	0.468	0.848	− 0.27106	2.0846	1

3.2 Model Development

As stated earlier, the Levenberg–Marquardt algorithm has been used to train the models. As the thermal conductivity and viscosity values were determined for concentrations and temperatures only, the input layer and output layer contained 2 and 1 neurons, respectively.

$$k_{nf} = f(\emptyset, T) \tag{2}$$

$$\mu_{nf} = f(\emptyset, T). \tag{3}$$

As stated earlier, the optimum number of neurons in the hidden layer was found through the trial and error method. The performance of the model was assessed for various activation functions such as sigmoid, hyperbolic tangent, and rectified linear. The sigmoid activation function was found to be outperforming other activation functions. Therefore, sigmoid was used to develop the model. This activation function is given as

$$Sigmoid: \quad f(z) = \frac{1}{1 + e^{-z}}, \tag{4}$$

where z represents the input to the hidden layer neurons.

The following steps were followed to reach to the optimum models:

1. Feeding model the normalized training data (80 % of the total data set).
2. Setting the number of neurons to 2.
3. Assessing the model performance on training data.
4. Assessing the model performance on testing data (normalized).
5. If unsatisfied performance, increasing the number of neurons.
6. Accessing the model performance on training data and test data.
7. Repeating steps 5 and 6 to get the optimum model.

In this work, three statistical parameters were used to evaluate the models' performance. These parameters were mean square error (MSE), mean absolute error (MAE), and coefficient of determination (R^2). These parameters are given as follows:

$$MSE = \frac{1}{n} \sum_{i=1}^{n} (V_e - V_n)^2 \tag{5}$$

$$MAE = \frac{1}{n} \sum_{i=1}^{n} |V_e - V_n| \tag{6}$$

$$R^2 = 1 - \frac{\sum_{i=1}^{n} (V_e - V_n)^2}{\sum_{i=1}^{n} (V_e - \overline{V_e})^2}, \tag{7}$$

where V, V, V_e, and n represent experimental value, neural network predicted value, average of experimental value, and total number of data points, respectively.

The relative deviation (RD) between experimental values and ANN predicted values was also determined. This was calculated as follows:

$$\text{Relative Deviation (\%)} = \frac{V_e - V_n}{V_e} \times 100.$$

(8)

4 Results and Discussion

4.1 Experimental

4.1.1 Thermal Conductivity

Figure 3 shows the variation of thermal conductivity with temperature (25 °C to 60 °C) for various MXene concentrations (0 mass% to 0.2 mass%). As can be seen from the figure, thermal conductivity of aqueous IoNanofluid increases as temperature and MXene concentration increases. It also shows that the thermal conductivity of aqueous ionic liquid can be increased from 0.468 W/m-K to 0.848 W/m-K (approx. 81 %) by adding 0.2 mass% MXene and increasing the temperature from 25 °C to 60 °C.

The variation of thermal conductivity with temperature and concentration can be reasoned by the concept of Brownian motion and percolation effect [42, 43]. The Brownian motion is the random motion of nanoparticles suspended in the IoNanofluid, which intensifies as temperature rises. The percolation effect can be defined as a phenomenon that occurs as nanoparticle to nanoparticle distance is reduced and
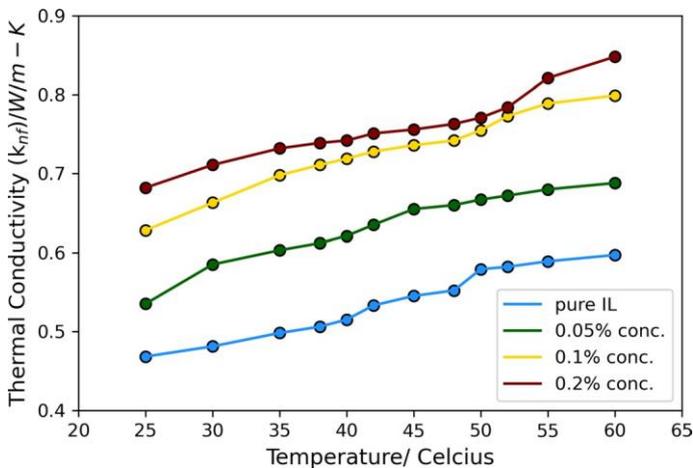
Fig. 3 Thermal conductivity of aqueous IoNanofluid for various temperatures and concentrations

results in particles colliding more frequently. For IoNanofluid at low temperatures, mainly the percolation effect contributes to an increase in thermal conductivity. At high temperatures, besides the percolation effect, nanoparticles also exhibit more Brownian motion owing to more energy content. This increases the frequency of collision even more. Hence, the thermal conductivity increases as temperature and concentration increases.

Figure 4 shows the variation of thermal conductivity ratio (TCR) with temperature (25 °C to 60 °C) for various MXene concentrations (0.05 mass% to 0.2 mass%). Although thermal conductivity is increasing as the temperature is increased, thermal conductivity ratio is not following any trend with temperature. This may be attributed to the uneven rate of increment of thermal conductivity of ionic liquid and IoNanofluids. The maximum TCR of 1.48 is achieved at 0.2 % concentration and 30 °C temperature.

4.1.2 Viscosity

Figure 5 shows the variation of viscosity with temperature (19.14 °C to 50.15 °C) for various MXene concentrations (0 mass% to 0.2 mass%). As can be seen from the figure, the viscosity of aqueous IoNanofluid decreases as temperature is increased and increases as concentration is increased. The figure also shows that, for the studied concentrations, viscosity can be reduced by over 42 % by increasing the temperature from 19.14 °C to 50.15 °C.

The variation of viscosity of developed IoNanofluid with temperature and MXene concentration can be reasoned as follows [44, 45]:

1. With concentration: Viscosity is the measure of internal resistance of the liquid to flow, which is a function of intermolecular forces. As nanoparticles are solid
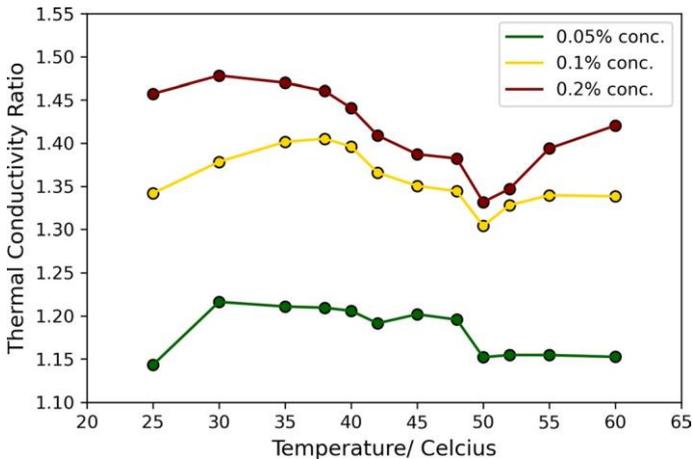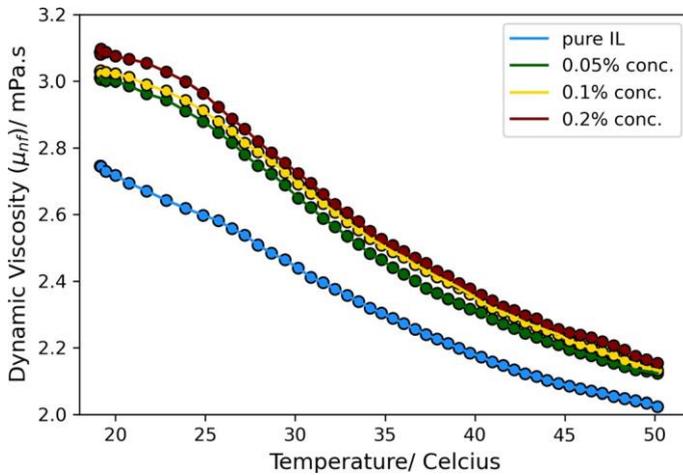

Fig. 4 Thermal conductivity ratio variation with temperature for various concentrations
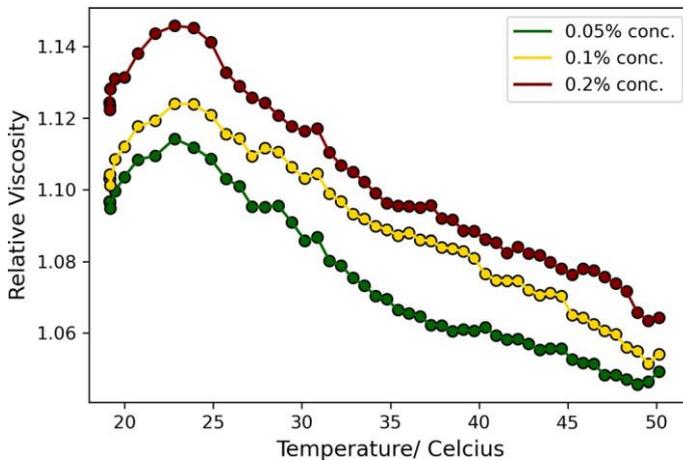
Fig. 5 Viscosity variation with temperature for various concentrations

and denser than ionic liquid, their addition in ionic liquid increases overall inter-molecular interactions. Thus, with MXene addition, viscosity increases.

2. With temperature: Intermolecular forces are a function of temperature. As temperature increases, intermolecular forces between MXene nanomaterials decrease (as intermolecular distance increases). Thus, viscosity decreases as temperature increases.

Figure 6 shows the variation of relative viscosity (RV) with temperature (19.14 °C to 50.15 °C) for various MXene concentrations (0.05 mass% to 0.2 mass%). Unlike thermal conductivity ratio, relative viscosity can be seen to have following

Fig. 6 Relative viscosity variation with temperature for various concentrations

a trend with temperature (for all concentrations) as relative viscosity is increas- ing initially and then decreasing. The maximum RV of 1.145 is achieved at 0.2 % concentration and approx. 23 °C temperature.

4.2 MLR Analysis of Thermal Conductivity and Viscosity

Multiple linear regression (MLR) analysis is often considered as an important step before developing more complex ANN models. The MLR analysis helps in analyzing various things such as the dependency of output on input variables. Besides, if the relationship between output and inputs is linear (or even near lin- ear), developing MLR is much more convenient. In point of fact, ANN models are only to be developed when relationship between inputs and output is non- linear and/or complex. Thus, MLR analysis is important to conduct before devel- oping more complex ANN models.

The data were first divided into training data (80 %) and test data (20 %). Then the data were used as such (without normalization) to do the MLR analysis. The following relations were obtained for thermal conductivity and viscosity:

$$TC = 0.0042407\,T + 1.05339621\varnothing + 0.38545 \tag{9}$$

$$\text{Viscosity} = 1.0911205\varnothing - 0.03016966T + 3.451877389. \tag{10}$$

To do the performance analysis of these relations obtained through MLR, indices described by Eqs. 5, 6, 7, and 8 were used. Table 5 describes the values of these indices for thermal conductivity and viscosity relation.

From the table, it can be inferred that the MLR's performance on thermal con- ductivity is poor, and is not able to give accurate thermal conductivity values. For viscosity, performance is better in comparison to thermal conductivity, but devia- tions are large. This shows that viscosity dependency on input variables is more linear in comparison to thermal conductivity. However, low performances of both the MLR models necessitate the development of more accurate ANN models.

Table 5 The performance of the thermal conductivity and viscosity MLR model on training data and test data

| Data	MSE	MAE	R^2	Minimum absolute RD	Maximum absolute RD	Mean absolute RD
Thermal conductivity						
Train	1.17E−03	2.977E−02	0.8843	0.303	8.307	4.548
Test	1.43E−03	3.3688E−02	0.7936	1.7	9.2	5.212
Viscosity						
Train	4.58E−03	5.58E−02	0.9518	0.019	6.1	2.241
Test	6.15E−03	6.526E−02	0.934	0.069	5.834	2.563

4.3 ANN Modeling

After experimentally determining the thermal conductivity and viscosity of pure IL and IoNanofluid, the data were used to develop the models. The optimum model was determined on the basis of the performance of the model on the training data and testing data. On the basis of performance, model can be classified as follows [46]:

1. Underfit: A model is underfit when model's performance is poor on training data as well as on test data.
2. Well fit: A well-fit model is a model which shows good and comparable performance on both training data and test data.
3. Overfit: A model is overfit when model's performance is far better on the training data than it is on test data. In other words, model's generalization capability is poor.

It is important to understand that the number of neurons greatly affects the generalization capability of ANN models. This makes analysis of model's performance (on training data and test data) very important. The total number of data points determined experimentally for thermal conductivity and viscosity were 48 and 200, respectively.

4.3.1 Thermal Conductivity

Figure 7 shows the variation of mean square error (MSE) with number of neurons for thermal conductivity ANN model. As can be seen from the figure, for 2 and 3 neurons in hidden layer, the model is underfit. As the number of neurons increases from 5 to 8, model can be seen to get overfitted. This can be said because even as
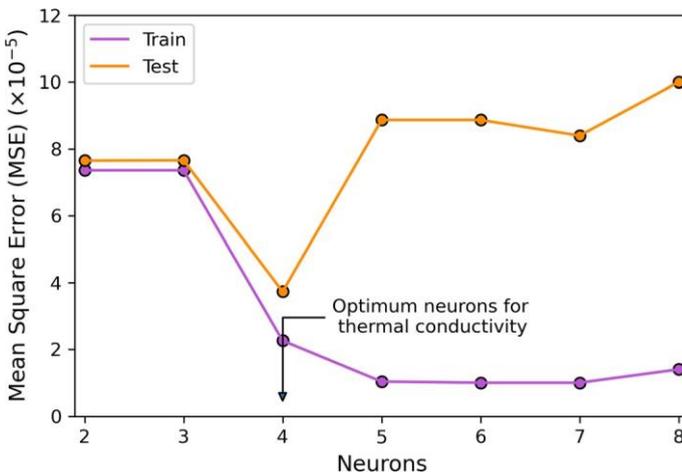
Fig. 7 Variation of mean square error with number of neurons in hidden layer for thermal conductivity model
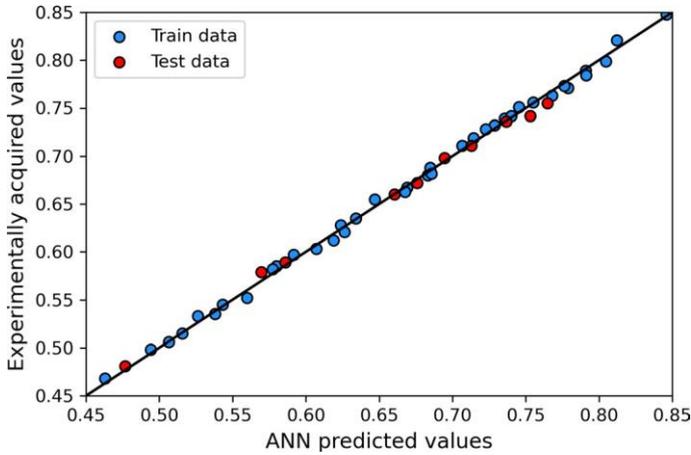
Fig. 8 Comparison between experimentally acquired thermal conductivity values and their ANN predictions

Table 6 The performance of the thermal conductivity model on training data and test data

Data	MSE	MAE	R^2	Minimum absolute RD	Maximum absolute RD	Mean absolute RD
Train	2.26E−05	4.23E−03	0.9977	0.074	1.421	0.646
Test	3.73E−05	4.85E−03	0.9946	0.08	1.644	0.741

the error on training data is reducing, error on test data is increasing. Figure also shows that error on test data is minimum for 4 neurons in hidden layer. Therefore, the optimum model was chosen to have the structure of 2-4-1 (input neurons-hidden neurons-output neuron).

Figure 8 shows the comparison between actual values and values predicted by the optimum thermal conductivity ANN model. The figure shows a line equidistant from both the axes. This means that a point lying on the line is also equidistant from the axes. As can be seen from the figure, nearly all the values are lying close to the line. The figure also compares the ANN predictions for training data and test data. As can be inferred, the predictions for training data (colored in blue) are more accurate when compared to test data (colored in red). However, this is acceptable as training errors are always lower than test errors.

Table 6 shows the value of MSE, MAE, R^2, and absolute RD (minimum, maximum, and mean) for training data and test data. As can be seen, difference in the values of these parameters for training data and test data is marginal. On this basis, it can be said that the model is a well-fit model.

Figure 9 shows the variation of RD with the temperature for training data (blue scatter points) and test data (red scatter points). As can be observed from the figure, there is no trend between RD and temperature. Further, maximum RD shown by model on training data is − 1.421 % at 48 °C. For testing data, maximum error is 1.644 %, which occurred at 50 °C.
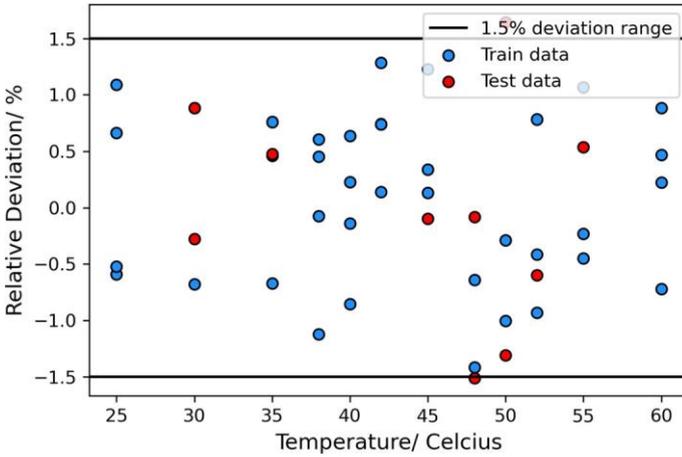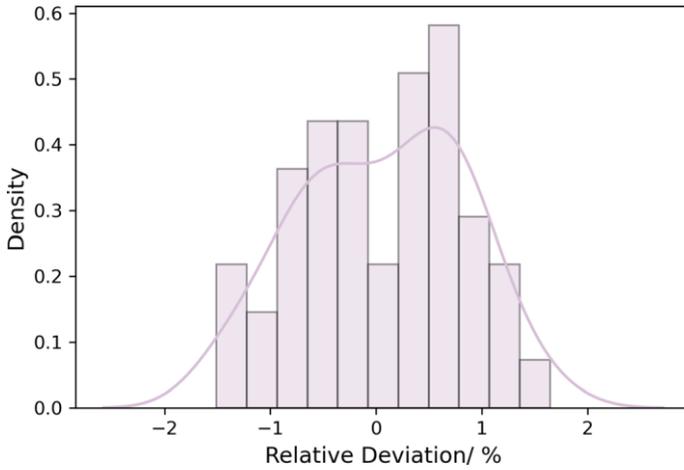
Fig. 9 The variation of relative deviation of thermal conductivity ANN model with temperature

Figure 10 shows the variation of RD with the MXene concentration for training data and test data. As can be observed, the model shows best performance for 0.2 % concentration. The model shows maximum error for pure IL (for both training data and test data). Also, both Figs. 9 and 10 show that 95.8 % of errors are in the range of ±1.5 % error.

Figure 11 shows the histogram and kernel density estimation of relative devia- tion of thermal conductivity ANN model. It can be inferred from the plot that the error on most of the data points lies in ± 1 % range, and also that most errors are away from maximum error.
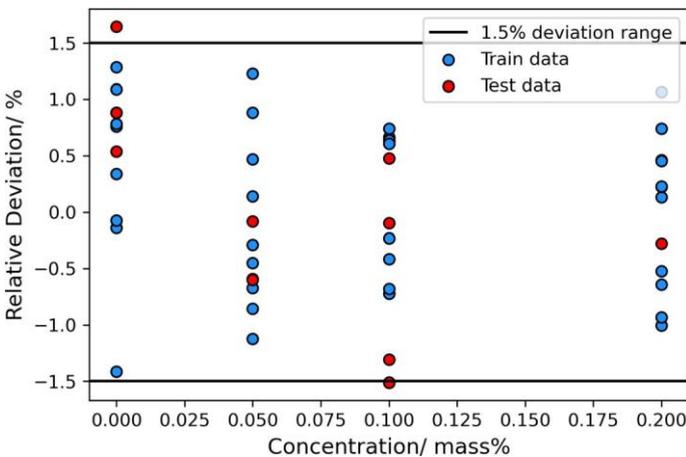
**Fig. 10** The variation of relative deviation of thermal conductivity ANN model with MXene concentration

**Fig. 11** The histogram of the relative deviation of thermal conductivity ANN model

On comparing the values of statistical indices for ANN model and MLR model, one can infer that ANN shows a significant improvement in prediction capabilities over MLR model.

4.3.2 Viscosity

Figure 12 shows the variation of mean square error (MSE) with number of neu- rons for viscosity ANN model. From the figure, we can observe that for 2, 3, and 4 neurons in hidden layer, the model is underfit and shows poor performance. As the number of neurons increases, model can be seen to have showing relatively good
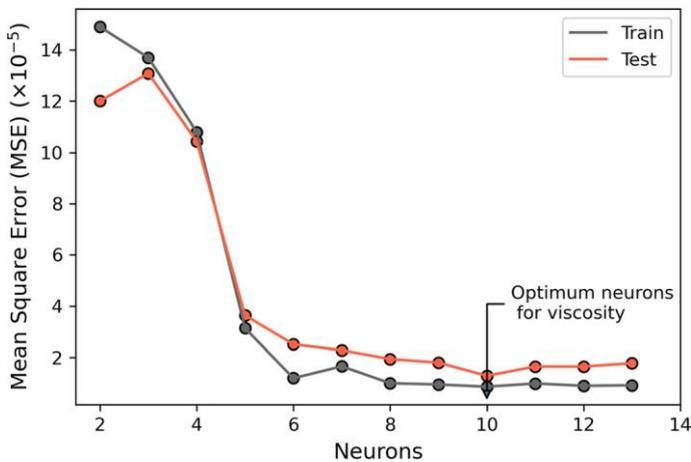
Fig. 12 Variation of mean square error with number of neurons in hidden layer for viscosity model
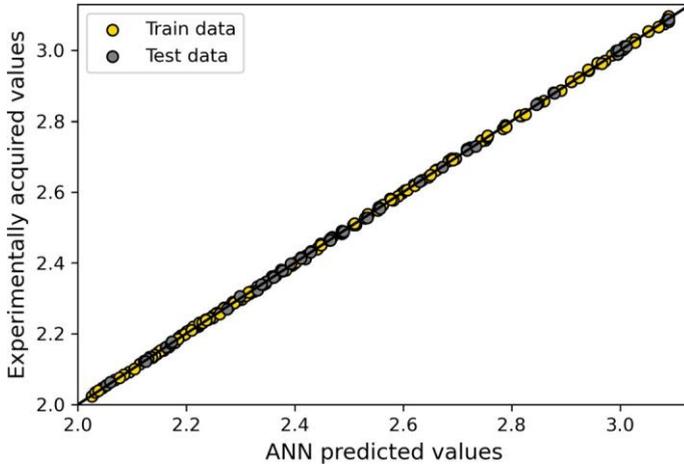
Fig. 13 Comparison between experimentally acquired viscosity values and their ANN predictions

Table 7 The performance of the viscosity model on training data and test data

Data	MSE	MAE	R^2	Minimum absolute RD	Maximum absolute RD	Mean absolute RD
Train	8.651E−06	2.45E−03	0.99990	0.0006	0.278	0.0942
Test	1.29E−05	2.77E−03	0.99986	0.005	0.3246	0.10995

performance. This signifies that model has started to map the relationship between inputs and output efficiently. As the number of neurons increases from 7 to 10, both training error and test error are reducing. However, as the number of neurons is increased further, the model can be seen to get slightly overfitted. Here, unlike the thermal conductivity model, the model is getting only slightly overfitted. As the error was the least at 10 neurons, the optimum model was chosen to have the struc- ture of 2-10-1.

Figure 13 shows the comparison between actual values and values predicted by the optimum viscosity ANN model. This figure also shows a line equidistant from both the axes. It can be observed from the figure that points are lying more closer to the line (when compared to thermal conductivity model). This signifies higher accuracy of the viscosity model. Also, predictions of the viscosity model on the test data can be observed to be more accurate. This signifies better generalization capability of viscosity model.

Table 7 shows the value of MSE, MAE, R^2, and absolute RD (minimum, maximum, and mean) for training data and test data. Here again it can be seen that the performance of the model on the training data and test data is almost same, confirming the good generalization capability of the viscosity model.

Figure 14 shows the variation of RD with the temperature for training data (yellow scatter points) and test data (gray scatter points). Here also, there is no trend between RD and temperature. The maximum RD shown by the model on training
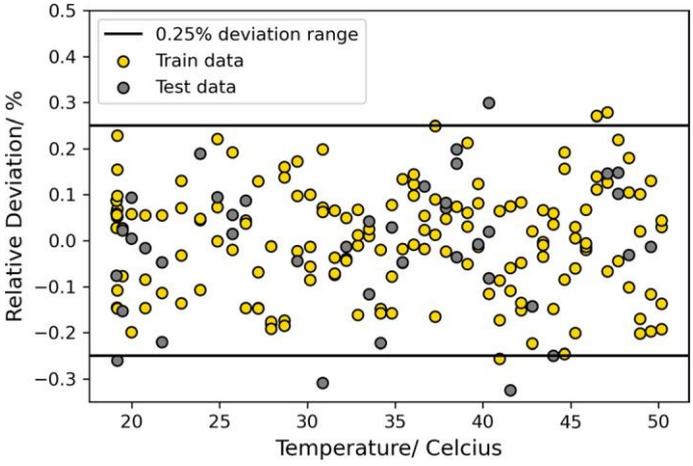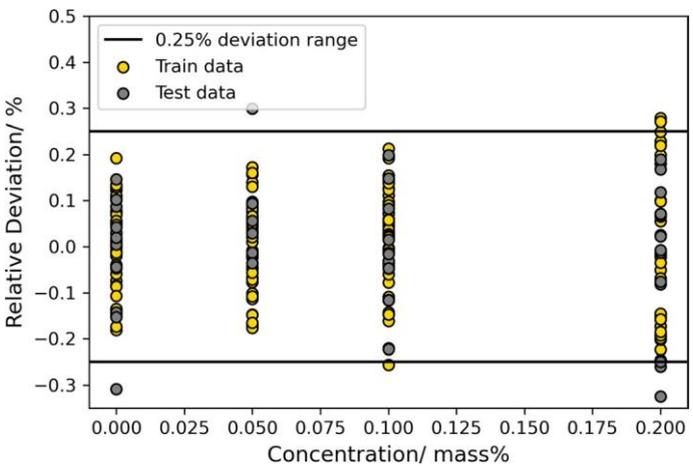
Fig. 14 The variation of relative deviation of viscosity ANN model with temperature

data is 0.278 % at 47.08 °C. For testing data, maximum error is − 0.3246 % at the temperature of 41.56 °C.

Figure 15 shows the variation of RD with the MXene concentration for training data and test data. It can be observed from the figure that model shows comparatively good performance for 0.1 % concentration. The maximum error shown for training data is 0.278 % at 0.2 % concentration, whereas maximum error shown for test data is − 0.3246 % at the same concentration. Also, both Figs. 14 and 15 show that around 96 % of errors are in the range of ± 0.25 % error.

Figure 16 shows the histogram and kernel density estimation of relative deviation of the viscosity ANN model. It can be seen from the plot that the maximum

Fig. 15 The variation of relative deviation of viscosity ANN model with MXene concentration
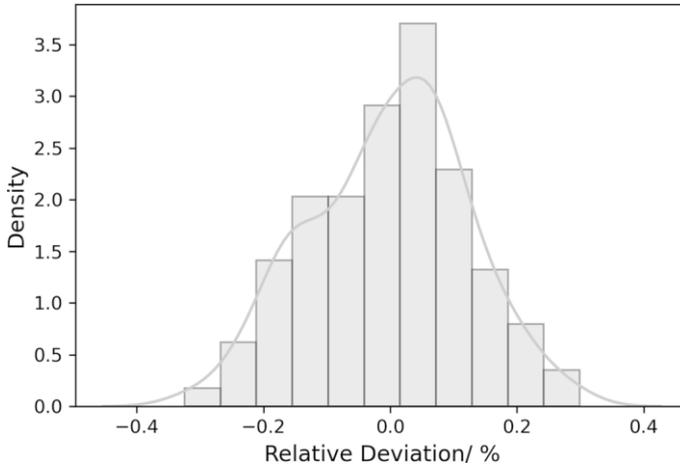
Fig. 16 The histogram of the relative deviation of viscosity ANN model

percentage of error lies in the range of ±0.1%. It also shows that the points lying near zero deviation are more when compared to the thermal conductivity model.

For viscosity also, performance of ANN model is much superior when compared to the performance of the MLR model. This can be attributed to more complex algorithm employed by ANNs.

5 Conclusions

In this work, our main objective was to develop the ANN models to predict the values of thermal conductivity and viscosity of MXene-doped [MMIM][DMP] ionic liquid. Firstly, MXene nanomaterial was synthesized and then used to prepare IoNanofluid with 0.05, 0.1, and 0.2 mass% concentration. The SEM analysis revealed the size of the developed nanomaterial to be less than 100 nm. In the study, the temperature was varied from 19 °C to 60 °C. Besides ANN models, two MLR models were also developed. The findings of our investigation are as follows:

– The experimental investigation on thermal conductivity and viscosity revealed that both temperature and concentration have a noteworthy impact on these properties. The maximum enhancement in the thermal conductivity was found to be 1.48 at 0.2 mass% concentration and 30 °C. For viscosity, maximum enhancement was 1.145 at 0.2 mass% and 23 °C temperature. Further, the investigation revealed that thermal conductivity could be increased by approximately 81 % by doping 0.2 mass% of MXene and increasing temperature to 60 °C. Moreover, viscosity could be reduced by an average of 42 % by increasing the temperature to 50.15 °C.
– The MLR models were developed for thermal conductivity and viscosity. The values of the coefficient of determination for thermal conductivity model and

viscosity model were 0.8843 and 0.9518, respectively. These values also revealed that viscosity's dependence on inputs is more linear when compared to thermal conductivity. On analyzing other statistical indices for both the models, it was concluded that the performances of the models were not accurate enough.

– The feedforward network was trained by the Levenberg–Marquardt algorithm. The trial and error method was used to determine the optimum neurons in the hidden layer. The optimum neurons for thermal conductivity model and viscosity model were found to be 4 and 10, respectively. With the help of statistical indices, both the models were found to be well-fit models. The values of MSE, MAE, and R for thermal conductivity and viscosity model were found to be $2.26E{-}05$, $4.23E{-}03$, and 0.9977; and $8.651E{-}06$, $2.45E{-}03$, and 0.9999, respectively. For thermal conductivity model, the maximum RD was 1.644 %, whereas for viscosity model, this figure was just -0.3246 %. Further, 95.8 % of the errors of thermal conductivity model were in the range of $\pm$ 1 %, whereas for viscosity model, 96 % of the errors were in the range of $\pm$ 0.25 %.

Compliance with Ethical Standards

Conflict of interest The authors declare that they have no competing interest.

References

1. D. Wen, G. Lin, S. Vafaei, K. Zhang, Review of nanofluids for heat transfer applications. Particuology **7**, 141–50 (2009)
2. C.A. Nieto de Castro, M.J.V. Lourenço, A.P.C. Ribeiro, E. Langa, S.I.C. Vieira, P. Goodrich, C. Hardacre, Thermal properties of ionic liquids and IoNanofluids of imidazolium and pyrrolidinium liquids. J. Chem. Eng Data **55**, 653–61 (2010)
3. S.U.S. Choi, J.A. Eastman, Enhancing thermal conductivity of fluids with nanoparticles. ASME Fluids Eng Div. **231**, 99–105 (1995)
4. M.A. Nazari, M.H. Ahmadi, M. Sadeghzadeh, M.B. Shafii, M. Goodarzi, A review on application of nanofluid in various types of heat pipes. J Cent. South Univ. **26**, 1021–41 (2019)
5. I.A. Qeays, S.M. Yahya, M. Asjad, Z.A. Khan, Multi-performance optimization of nanofluid cooled hybrid photovoltaic thermal system using fuzzy integrated methodology. J Clean. Prod. **256**, 120451 (2020)
6. I.A. Qeays, S.M. Yahya, M.S.B. Arif, A. Jamil, Nanofluids application in hybrid photovoltaic thermal system for performance enhancement: a review. AIMS Energy **8**, 365–93 (2020)
7. N. Ali, J.A. Teixeira, A. Addali, A review on nanofluids: fabrication, stability, and thermophysical properties. J Nanomater. **2018**, 6978130 (2018)
8. L. Qiu et al., A review of recent advances in thermophysical properties at the nanoscale: from solid state to colloids. Phys. Rep. **843**, 1–81 (2020)

9. S.K. Singh, A.W. Savoy, Ionic liquids synthesis and applications: an overview. J. Mol. Liq. **297**, 112038 (2020)

10. A.A. Minea, S.M.S. Murshed, A review on development of ionic liquid based nanofluids and their heat transfer behavior. Renew. Sustain. Energy Rev. **91**, 584–99 (2018)

11. R.D. Rogers, K.R. Seddon, Ionic liquids-solvents of the future? Science **302**, 792–3 (2003)

12. K. Paduszyński, U. Domańska, Viscosity of ionic liquids: an extensive database and a new group contribution model based on a feed-forward artificial neural network. J. Chem. Inf. Model. **54**, 1311–24 (2014)

13. J.F. Wishart, Energy applications of ionic liquids. Energy Environ. Sci. **2**, 956–61 (2009)

14. R. Ratti, Ionic liquids: synthesis and applications in catalysis. Adv. Chem. **2014**, 729842 (2014)

15. R.L. Vekariya, A review of ionic liquids: applications towards catalytic organic transformations. J. Mol. Liq. **227**, 44–60 (2017)

16. W. Dai, W. Yang, Y. Zhang, D. Wang, X. Luo, X. Tu, Novel isothiouronium ionic liquid as efficient catalysts for the synthesis of cyclic carbonates from CO_2 and epoxides. J. Carbondioxide Util. **17**, 256–262 (2017)

17. N. Sugihara, K. Nishimura, H. Nishino, S. Kanehashi, K. Mayumi, Y. Tominaga, T. Shimomura, K. Ito, Ion-conductive and elastic slide-ring gel Li electrolytes swollen with ionic liquid. Electro Acta. **229**, 166–72 (2017)

18. E.A. Chernikova, L.M. Glukhov, V.G. Krasovskiy, L.M. Kustov, M.G. Vorobyeva, A.A. Koroteev, Ionic liquids as heat transfer fluids: comparison with known systems, possible applications, advantages and disadvantages. Russ. Chem. Rev. 84, 875–90 (2015)

19. V.V. Wadekar, Ionic liquids as heat transfer fluids—an assessment using industrial exchanger geometries. Appl. Therm. Eng. **111**, 1581–7 (2017)

20. M. Watanabe, M.L. Thomas, S. Zhnag, K. Ueno, T. Yasuda, K. Dokko, Application of ionic liquids to energy storage and conversion materials and devices. Chem. Rev. **117**, 7190–239 (2017)

21. J.M.P. França, M.J.V. Lourenço, S.M.S. Murshed, A.A.H. Pádua, C.A. de Nieto Castro, Thermal conductivity of ionic liquids and ionanofluids and their feasibility as heat transfer fluids. Indus Eng. Chem. Res. **57**, 6516–29 (2018)

22. F.F. Zhang, F.F. Zheng, X.H. Wu, Y.L. Yin, G. Chen, Variations of thermophysical properties and heat transfer performance of nanoparticle-enhanced ionic liquids. R. Soc. Open Sci. **6**, 182040 (2019)

23. B. Bakthavatchalam, K. Habib, R. Saidur, B.B. Saha, K. Irshad, Comprehensive study on nanofluid and ionanofluid for heat transfer enhancement: a review on current and future perspective. J. Mol. Liq. **305**, 112787 (2020)

24. A.A. Minea, Overview of ionic liquids as candidates for new heat transfer fluids. Int. J. Thermophys. **41**, 151 (2020)

25. G. Huminic, A. Huminic, Heat transfer capability of ionanofluids for heat transfer applications. Int. J. Thermophys. **42**, 12 (2020)

26. E.I. Chereche̦s, J.I. Prado, M. Chereche̦s, A.A. Minea, L. Lugo, Experimental study on thermophysical properties of alumina nanoparticle enhanced ionic liquids. J. Mol. Liq. **291**, 111332 (2019)

27. T.C. Paul, A.K.M.M. Morshed, E.B. Fox, J.A. Khan, Thermal performance of Al_2O_3 Nanoparti-cle Enhanced Ionic Liquids (NEILs) for Concentrated Solar Power (CSP) applications. Int. J. Heat Mass Transf. **85**, 585–94 (2015)

28. T.C. Paul, A.K.M.M. Morshed, J.A. Khan, Nanoparticle enhanced ionic liquids (NEILs) as working fluid for the next generation solar collector. Procedia Eng. **56**, 631–6 (2013)

29. F. Wang, L. Han, Z. Zhang, X. Fang, J. Shi, W. Ma, Surfactant-free ionic liquid-based nanofluids with remarkable thermal conductivity enhancement at very low loading of graphene. Nano Res. Lett. **7**, 314 (2012)

30. H. Xie, Z. Zhao, J. Zhao, H. Gao, Measurement of thermal conductivity, viscosity and density of ionic liquid [EMIM][DEP]-based nanofluids. Chin. J. Chem. Eng. **24**, 331–8 (2016)

31. R.M. Ronchi, J.T. Arantes, S.F. Santos, Synthesis, structure, properties and applications of MXenes: current status and perspectives. Ceram. Int. **45**, 18167–88 (2019)

32. Z. Bao, N. Bing, X. Zhu, H. Xie, W. Yu, Ti3C2Tx MXene contained nanofluids with high ther- mal conductivity, super colloidal stability and low viscosity. Chem. Eng. J. (2020). https://doi.org/10.1016/j.cej.2020.126390

33. N. Aslfattahi, L. Samylingam, A.S. Abdelrazik, A. Arifutzzaman, R. Saidur, MXene based new class of silicone oil nanofluids for the performance improvement of concentrated photovoltaic ther- mal collector. Solar Energy Mater. Solar Cells. **211**, 110526 (2020)

34. D. Toghraie, M.H. Aghahadi, N. Sina, F. Soltani, Application of Artificial Neural Networks (ANNs) for predicting the viscosity of tungsten oxide (WO3)-MWCNTs/engine oil hybrid nanofluid. Int. J. Thermophys. **41**, 163 (2020)

35. M. Sadi, Prediction of thermal conductivity and viscosity of ionic liquid based nanofluid using adaptive neuro fuzzy inference system. Heat Transf. Eng. **38**, 1561–72 (2017)

36. L. Das, K. Habib, R. Saidur, N. Aslfattahi, S.M. Yahya, F. Rubbi, Improved thermophysical properties and energy efficiency of aqueous ionic liquid/MXene nanofluid in a hybrid PV/T solar system. Nanomaterials **10**, 1372 (2020)

37. S. Rostami, R. Kalbasi, N. Sina, A.S. Goldanlou, Forecasting the thermal conductivity of a nanofluid using artificial neural networks. J. Therm. Anal. Calorim. (2020). https://doi.org/10.1007/s10973-020-10183-2

38. M. Bahiraei, S. Nazari, H. Moayedi, H. Safarzadeh, Using neural network optimized by imperialist competition method and genetic algorithm to predict water productivity of a nanofluid-based solar still equipped with thermoelectric modules. Powder Technol. **366**, 571–86 (2020)

39. B. Paknezhad, M. Vakili, M. Bozorgi, M. Hajialibabaie, M. Yahyaei, A hybrid genetic-BP algorithm approach for thermal conductivity modeling of nanofluid containing silver nanoparticles coated with PVP. J. Therm. Anal. Calorim. (2020). https://doi.org/10.1007/s10973-020-09989-x

40. H. Kalani, M. Sardarabadi, M. Passandideh-Fard, Using artificial neural network models and particle swarm optimization for manner prediction of a photovoltaic thermal nanofluid based collector. Appl. Therm. Eng. **113**, 1170–7 (2017)

41. M.R.H. Jirandeh, M. Mohammadiun, H. Mohammadiun, M.H. Dubaie, M. Sadi, Intelligent modeling of rheological and thermophysical properties of nanoencapsulated PCM slurry. Heat Transf. **49**, 2080–102 (2020)

42. C.C. Li, N.Y. Hau, Y. Wang, A.K. Soh, S.P. Feng, Temperature-dependent effect of percolation and Brownian motion on the thermal conductivity of TiO2-ethanol nanofluids. Phys. Chem. Chem. Phys. **18**, 15363–8 (2016)

43. M.U. Sajid, H.M. Ali, Thermal conductivity of hybrid nanofluids: a critical review. Int. J. Heat Mass Transf. **126**, 211–34 (2018)

44. A.D. Zadeh, D. Toghraie, Experimental investigation for developing a new model for the dynamic viscosity of silver/ethylene glycol nanofluid at different temperatures and solid volume fractions. J. Therm. Anal. Calorim. **131**, 1449–61 (2018)

45. F. Jabbari, A. Rajabpour, S. Saedodin, Viscosity of carbon nanotube/water nanofluid. J. Therm. Anal. Calorim. **135**, 1787–96 (2019)

46. N. Parashar, N. Aslfattahi, S.M. Yahya, R. Saidur, An artificial neural network approach for the prediction of dynamic viscosity of MXene-palm oil nanofluid using experimental data. J. Therm. Anal. Calorim. (2020). https://doi.org/10.1007/s10973-020-09638-3